



1 **Land-sea coupling of Early Pleistocene glacial cycles in the southern North Sea exhibit**
2 **dominant Northern Hemisphere forcing**

3 Timme Donders^{1,2}, Niels A.G.M. van Helmond³, Roel Verreussel², Dirk Munsterman⁴, Johan
4 Ten Veen⁴, Robert P. Speijer⁵, Johan W.H. Weijers^{3*}, Francesca Sangiorgi³, Francien
5 Peterse³, Gert-Jan Reichart^{3,6}, Jaap Sinninghe Damsté^{3,6}, Lucas Lourens³, Gesa Kuhlmann⁷
6 and Henk Brinkhuis^{3,6}

7
8 ¹ Department of Physical Geography, Fac. of Geosciences, Utrecht University,
9 Heidelberglaan 2, 3584CD, Utrecht, The Netherlands.

10 ² TNO - Applied Geosciences, Netherlands Organisation of Applied Scientific Research
11 Princetonlaan 6, 3584 CB Utrecht, The Netherlands.

12 ³ Department of Earth Sciences, Fac. of Geosciences, Utrecht University, Heidelberglaan 2,
13 3584CS, Utrecht, The Netherlands.

14 ⁴ TNO - Geological Survey of the Netherlands, Netherlands Organisation of Applied
15 Scientific Research, Princetonlaan 6, 3584 CB Utrecht, The Netherlands.

16 ⁵ Department of Earth and Environmental Sciences, KU Leuven, 3001 Heverlee, Belgium

17 ⁶ NIOZ Royal Netherlands Institute for Sea Research, P.O. Box 59, 1790 AB, Den Burg,
18 Texel, The Netherlands

19 ⁷ BGR - Federal Institute for Geosciences and Natural Resources, Geozentrum Hannover
20 Stilleweg 2, D-30655 Hannover

21 * Currently at: Shell Global Solutions International B.V., Grasweg 31, 1031 HW, Amsterdam,
22 The Netherlands

23 Correspondence to: t.h.donders@uu.nl

24

25



26 **Abstract**

27 We assess the disputed phase relations between forcing and climatic response in the Early
28 Pleistocene with a spliced Gelasian (~2.6 – 1.8 Ma) multi-proxy record from the southern
29 North Sea. The cored sections couple climate evolution on both land and sea during the onset
30 of Northern Hemisphere Glaciations (NHG) in NW Europe, providing the first well-
31 constrained stratigraphic sequence of the classic terrestrial Praetiglian Stage. Terrestrial
32 signals were derived from the Eridanos paleoriver, a major fluvial system that contributed a
33 large amount of freshwater to the northeast Atlantic. Due to its latitudinal position, the
34 Eridanos catchment was likely affected by Early Pleistocene NHG, leading to intermittent
35 shutdown and reactivation of river flow and sediment transport. Here we apply organic
36 geochemistry, palynology, carbonate isotope geochemistry, and seismostratigraphy to
37 document both vegetation changes in the Eridanos catchment and regional surface water
38 conditions and relate them to Early Pleistocene glacial-interglacial cycles, and relative sea
39 level changes. Paleomagnetic and palynological data provide a solid integrated timeframe that
40 ties the obliquity cycles, expressed in the borehole geophysical logs, to Marine Isotope Stages
41 (MIS) 103 to 92, independently confirmed by a local benthic oxygen isotope record. Marine
42 and terrestrial palynological and organic geochemical records provide high resolution
43 reconstructions of relative Terrestrial and Sea Surface Temperature (TT and SST), vegetation,
44 relative sea level, and coastal influence.

45 During the prominent cold stages MIS 100, 98 and 96, the record indicates increased non-
46 arboreal vegetation, and low SST and TT, and low relative sea level. During the warm stages
47 MIS 99, 97 and 95 we infer freshwater influx increases causing stratification of the water
48 column together with higher % arboreal vegetation, high SST and relative sea level maxima.
49 The Early Pleistocene distinct warm-cold alterations are synchronous between land and sea,
50 but lead the relative sea level change. The record provides evidence for a dominantly NH



51 driven cooling and glacial build up which is obliquity driven. Timing of southward migration
52 of Arctic surface water masses, indicated by relative SST, are furthermore relevant for the
53 discussion on the relation between the intensity of the Atlantic meridional overturning
54 circulation and ice sheet growth in order to identify lead-lags between forcing and response of
55 Early Pleistocene glaciations.

56

57 **Keywords:** Glacial-interglacial climate, palynology; organic geochemistry; obliquity, land-
58 sea correlation, Eridanos delta, southern North Sea



59 **1 Introduction**

60 The build-up of extensive Northern Hemisphere (NH) land ice started around 3.6 Ma ago
61 (Ruddiman et al. 1986; Mudelsee and Raymo, 2005; Ravelo et al., 2004; Ravelo, 2010), with
62 stepwise intensifications between 2.7 and 2.54 Ma ago (e.g., Shackleton and Hall, 1984;
63 Raymo et al., 1989; Haug et al., 2005; Lisiecki and Raymo, 2005; Sosdian and Rosenthal,
64 2009). In the North Atlantic region the first large-scale Early Pleistocene glaciations, Marine
65 Isotope Stages (MISs) 100 - 96, are marked by e.g. appearance of ice-rafted debris and
66 southward shift of the Arctic front (see overview in Hennissen et al., 2015). On land, the
67 glaciations led to faunal turnover (e.g. Lister, 2004; Meloro et al., 2008) and widespread
68 vegetation changes (e.g. Zagwijn, 1992; Hooghiemstra and Ran, 1994; Svenning, 2003;
69 Brigham-Grette et al., 2013). Many theories have been put forward to explain the initiation of
70 these NH glaciations around the Plio-Pleistocene transition interval. Causes include tectonics
71 (Keigwin, 1982, Raymo, 1994; Haug and Tiedemann, 1998; Knies et al, 2004; Poore et al.,
72 2006), orbital forcing dominated by obliquity-paced variability (Hays et al., 1976; Maslin et
73 al., 1998; Raymo et al., 2006) and atmospheric CO₂ concentration decline (Pagani et al., 2010;
74 Seki et al., 2010; Bartoli et al., 2011) driven by e.g. changes in ocean stratification that
75 affected the biological pump (Haug et al., 1999). Changes were amplified by NH albedo
76 change (Lawrence et al., 2010), and possibly tropical atmospheric circulation change and
77 breakdown of permanent El Niño (Ravelo et al., 2004; Brierley and Fedorov, 2010; Etourneau
78 et al., 2010).

79

80 Key aspects in this discussion are the phase relations between temperature change on land, in
81 the surface and deep ocean, and ice sheet accretion (expressed through global eustatic sea
82 level lowering) in both Northern and Southern Hemispheres. According to Raymo et al.



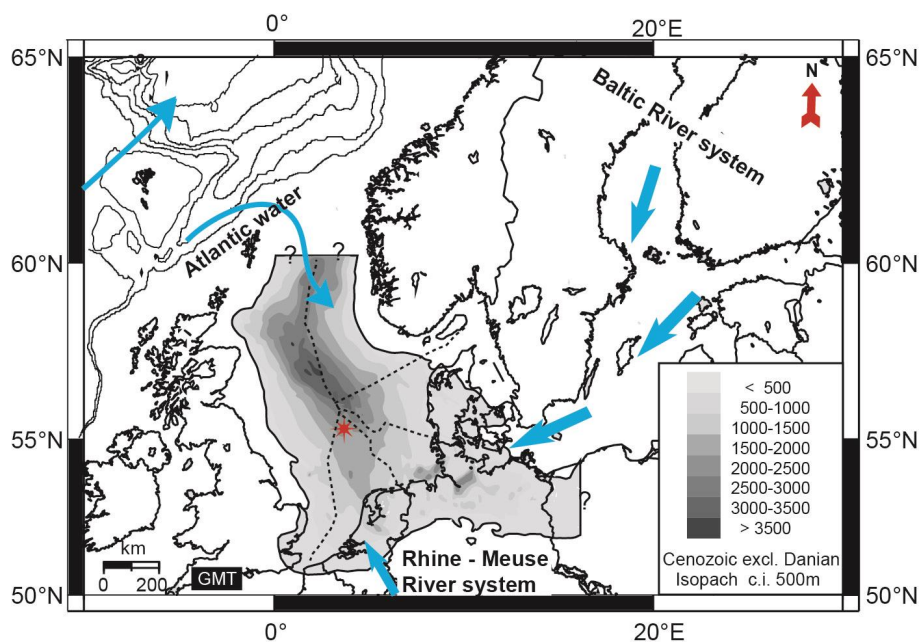
83 (2006), Early Pleistocene obliquity forcing dominated global sea level and $\delta^{18}\text{O}_{\text{benthic}}$, because
84 precession-paced changes in the Greenland and Antarctic ice sheets cancelled each other out.
85 In this view, climate records independent of sea level variations should display significant
86 variations on precession timescale. Alternatively, variations in the total integrated summer
87 energy, which is obliquity controlled, might be responsible for the dominant obliquity pacing
88 of the Early Pleistocene (Huybers, 2006; Tzedakis et al., 2017). The dominance of the
89 obliquity component has been attributed to feedbacks between high-latitude insolation, albedo
90 (sea-ice and vegetation) and ocean heat flux (Koenig et al., 2011; Tabor et al., 2014). Sosdian
91 and Rosenthal (2009) suggested that temperature variations, based on benthic foraminifer
92 magnesium/calcium (Mg/Ca) ratios from the North Atlantic, explain a substantial portion of
93 the global variation in the $\delta^{18}\text{O}_{\text{benthic}}$ signal. North Atlantic climate responses were closely
94 phased with $\delta^{18}\text{O}_{\text{benthic}}$ changes during the Early Pleistocene, suggesting a strong common NH
95 high latitude imprint on North Atlantic climate signals (Lawrence et al., 2010). Following this
96 reasoning, glacial build-up should be in phase with decreases in NH sea surface temperatures
97 (SST) and terrestrial temperatures (TT). To explicitly test this hypothesis we perform a high-
98 resolution multiproxy terrestrial and marine palynological, organic geochemical, and stable
99 isotope study on a marginal marine sediment sequence from the southern North Sea (SNS)
100 during the Early Pleistocene “41 kyr-world”. We investigate the leads and lags of regional
101 marine vs. terrestrial climatic cooling during MIS 102-92, and assess the local sea level
102 response relative to global patterns from the $\delta^{18}\text{O}_{\text{benthic}}$ stack of Lisiecki and Raymo (2005;
103 LR04). In addition, the record can better constrain the signature and timing of the regional
104 continental Praetiglian stage (Van der Vlerk and Florschütz, 1953; Zagwijn, 1960) that is still
105 widely used, but which stratigraphic position and original definition is questionable (Donders
106 et al., 2007; Kemna and Westerhoff, 2007).

107



108 2 Geological setting

109 During the Neogene the epicontinental North Sea Basin was confined by landmasses except
110 towards the northwest, where it opened into the Atlantic domain (Fig. 1) (Bijlsma, 1981;
111 Ziegler, 1990). Water depths in the central part were approximately between 100 to 300 m as
112 deduced from seismic geometry (Huuse et al., 2001; Overeem et al., 2001). In contrast, the
113 recent North Sea has an average depth between 20-50 m in the south that deepens only
114 towards the shelf edge towards 200 m in the north-west (e.g., Caston, 1979). From the
115 present-day Baltic region a formidable river system, known as the Eridanos paleoriver,
116 developed which built up the Southern North Sea delta across southern Scandinavia (Sørensen
117 et al., 1997; Michelsen et al., 1998; Huuse et al., 2001; Overeem et al., 2001).



118
119 *Figure 1: Geographical map of the North Sea region with the superimposed thickness of*
120 *Cenozoic sediment infill after Ziegler (1990) and the offshore sectors (stippled lines). The*
121 *different water types influencing the Pliocene North Sea hydrography including the*



122 *freshwater supply of the Baltic river system, the Rhine-Meuse river system and Atlantic*
123 *surface waters are indicated with black arrows. The location of the boreholes A15-3 (UTM X*
124 *552567.1, Y 6128751.6) and A15-4 (UTM X 557894.4, Y 6117753.5) is marked by an asterisk,*
125 *see also Fig. S1.*

126 This delta was characterized by an extensive distributary system that supplied large amounts
127 of freshwater and sediment to the shelf sea (Overeem et al., 2001), resulting in a sediment
128 infill of ~1500 m in the central North Sea Basin (Fig. 1). This system was fed by rainfall as
129 well as by melt-water originating from Scandinavian glaciers (Kuhlmann et al., 2004),
130 principally from the Baltic Shield in the east with some contribution from the south (Fig. 1)
131 (Bijlsma, 1981; Kuhlmann, 2004). The sedimentation rates reached up to 84 cm/kyr at the
132 studied locations (Fig. 2) (Kuhlmann et al., 2006b). Today, the continental river runoff
133 contributes only 0.5 % of the water budget in the North Sea (Zöllmer and Irion, 1996)
134 resulting in sedimentation rates ranging between 0.4 to 1.9 cm/kyr in the Norwegian Channel,
135 and 0.5 - 1 cm/kyr in the southern part of the North Sea (de Haas et al., 1997).

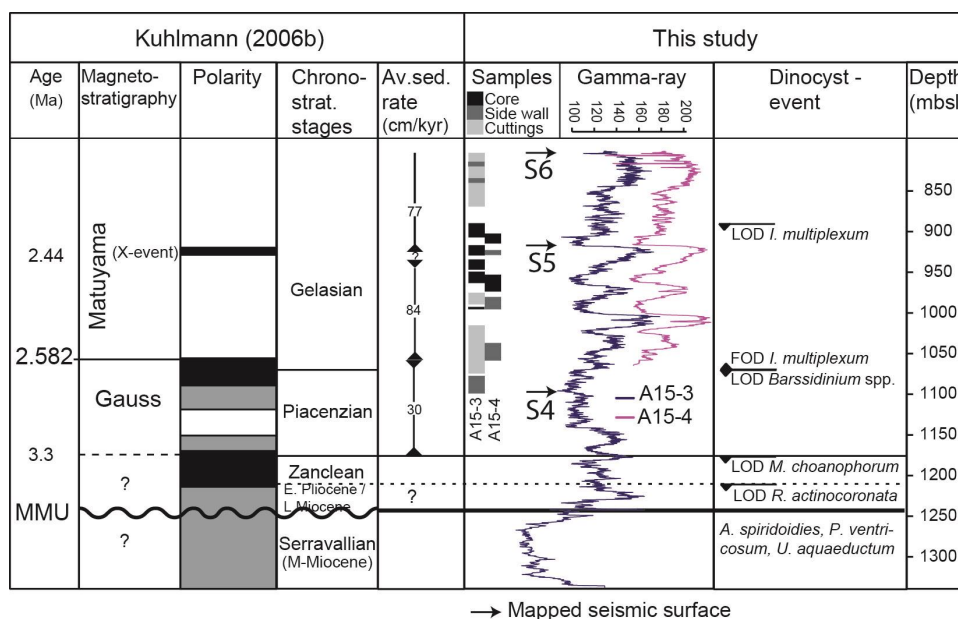
136

137 **3 Material, core description and age model**

138 Recent exploration efforts in the SNS led to the successful recovery of cored sedimentary
139 successions of marine isotope stages (MIS) 102-92 and continuous paleomagnetic logs (Fig.
140 2) (Kuhlman et al, 2006ab). An integrated age model is based on a multidisciplinary
141 geochronological analysis of several boreholes within the SNS (Kuhlmann et al., 2006ab) and
142 dinocyst biostratigraphy. The magnetostratigraphy and age-diagnostic dinocyst events used
143 for this age-model are summarized in Fig. 2. For quantitative palynological and geochemical
144 analyses, discrete sediment samples were taken from two exploration wells A15-3 and A15-4
145 located in the northernmost part of the Dutch offshore sector in the SNS at the Neogene
146 sedimentary depocentre (Fig. 1). The recovered material mainly consists of fine-grained, soft



147 sediments (clayey to very fine sandy), sampled from cuttings, undisturbed sidewall cores and
148 core sections (Fig. 2). Geochemical analyses were limited to the (sidewall) core intervals.
149 Clear cyclic variations in the gamma ray signal and associated seismic reflectors across the
150 interval can be correlated across the entire basin (Kuhlmann and Wong, 2008; Thöle et al.
151 2014). Samples from the two boreholes were spliced based on the gamma-ray logs (Fig. 2)
152 and biostratigraphic events to generate a composite record. The age model is mainly based on
153 the position of the Gauss-Matuyama transition at the base of log unit 6 correlating to the base
154 of MIS 103, and the identification of the X-event, which correlates the top of log unit 9 to
155 MIS 96 (Kuhlmann et al., 2006a,b) (Fig. 2). The depositional model by Kuhlmann and Wong
156 (2008) relates the relatively fine-grained, high gamma ray intervals to interglacials
157 characterized by river high run off. Around glacial terminations, when sea-level was low,
158 massive amounts of very fine-grained clayey to fine silty material were deposited in the basin,
159 the ultimate waste-products of intense glaciation. During warmer periods with high sea-level
160 more mixed, courser-grained sediments characterize the deposits, also reflecting a
161 dramatically changed hinterland, retreated glaciers, and possibly (stronger) bottom currents
162 (Kuhlmann and Wong, 2008). Based on this phase relation, detailed magneto- and
163 biostratigraphy, grain size measurements, and previous low resolution relative SST indices
164 (Kuhlmann et al., 2004; Kuhlmann et al., 2006a,b), the finer grained units are consistently
165 correlated to MIS 102 – 92. Based on this correlation, the sequence is here transferred to an
166 age scale based on the corresponding LR04 MIS transitions (Fig. S3).
167



168

169 *Figure 2: Chronology and mean sedimentation rates as derived from biostratigraphy and*
 170 *paleomagnetic data (Kuhlmann, 2006ab) in combination with the gamma-ray log of A15-3*
 171 *and A15-4 used in this study on a common depth scale. The position of various sample types*
 172 *and the mapped seismic horizons S4-6 (Fig. S1) are indicated. Material for the sidewall cores*
 173 *is limited, and used only for palynology and organic geochemistry. LOD/FOD: Last/First*
 174 *occurrence datum. LODs of M. choanophorum and R. actinocoronata are updated according*
 175 *to De Schepper et al. (2009).*

176

177 The regional structure and development of the delta front across the Plio-Pleistocene
 178 transition interval is very well constrained by a high-resolution regional geological model that
 179 represents the anatomy of the Eridanos (pro-) delta (Kuhlmann and Wong, 2008; Ten Veen et
 180 al., 2013). A total of 25 seismic horizons in the Plio-Pleistocene transition interval were
 181 mapped using series of publically available 2D and 3D seismic surveys across the northern
 182 part of the Dutch offshore sector. For all these surfaces the distribution of delta elements such
 183 as of topset-, foreset- and toset-to-prodelta has been determined, resulting in zonal maps (250



184 m grid size) that represent the present day geometry of the surfaces. The paleoenvironmental
185 reconstructions are compared to these maps to constrain the regional setting and aid the
186 interpretations.

187

188 **4 Paleoenvironmental proxies and methods**

189 *4.1 Benthic oxygen and carbon isotopes ($\delta^{18}O_b$ and $\delta^{13}C_b$)*

190 Oxygen and carbon isotopes were measured on tests of *Cassidulina teretis*, a cold water
191 species of endobenthic foraminifera that is generally abundant in the samples and common in
192 fine sediment and relatively low salinities (Mackensen and Hald, 1988; Rosoff and Corliss,
193 1992). Because of their endobenthic habitat, they record isotope compositions of pore waters,
194 which leads to somewhat reduced ($\delta^{13}C_b$) values compared to the overlying bottom waters.
195 Since the amount of material from the sidewall cores is limited, the isotope data is only
196 produced for the cored intervals with the principal aim to confirm the phase relationship
197 described by Kuhlmann and Wong (2008) between facies and climate. Between ~20 and 50
198 μg of specimen per sample was weighed after which the isotopes of the carbonate were
199 measured using a Kiel III device coupled to a 253 ThermoFinnigan MAT instrument. Isotope
200 measurements were normalized to an external standard ‘NBS-19’ ($\delta^{18}O = -2.20\%$, $\delta^{13}C =$
201 1.95%). Isotope data from specimens of poor to very poor preservation, due to
202 recrystallization and dissolution, particularly in MIS 96, were rejected.

203

204 *4.2 Palynological proxies*

205 In modern oceans, dinoflagellates are an important component of the (phyto-)plankton. About
206 15-20% of the marine dinoflagellates form an organic walled cyst (dinocyst) during the life
207 cycle that can be preserved in sediments (Head, 1996). Dinocyst distribution in marine surface
208 sediments has shown to reflect changes in the sea surface water properties, mostly responding



209 to temperature (e.g., Rochon et al., 1999; Zonneveld et al., 2013). Down-core changes in
210 dinocyst assemblages is a widely used and successful tool for reconstructing past
211 environmental changes especially in the Quaternary (e.g., De Vernal et al., 2009). However,
212 paleoecology of Paleogene, Miocene and Pliocene fossil dinocysts has also been established
213 in the last years (e.g., Versteegh and Zonneveld, 1994; Head et al., 2004; Pross and Brinkhuis,
214 2005; Sluijs et al., 2005; Schreck et al., 2013; De Schepper et al., 2011; 2013; Hennissen et
215 al., 2017).

216

217 Here we use the preference of certain taxa to cold-temperate to arctic surface waters to derive
218 sea surface temperature (SST) trends. The cumulative percentage of the dinocysts *Filisphaera*
219 *microornata*, *Filisphaera filifera*, *Filisphaera sp.*, *Habibacysta tectata* and *B. tepikiense* on
220 the total dinocysts represents our cold surface water indicator (Versteegh and Zonneveld,
221 1994; Donders et al., 2009; De Schepper et al., 2011). Interestingly, *Bitectatodinium*
222 *tepikiense*, the only extant dinocyst among our cold-water loving species, has been recorded
223 from the mixing zone of polar front oceanic waters with cold brackish meltwaters from
224 glacier ice (e.g., Bakken and Dale, 1986) and at the transition between the subpolar and
225 temperate zones (Dale, 1996). The combined abundance of *Lingulodinium machaerophorum*,
226 *Tuberculodinium vancampoeae*, *Polysphaeridium zoharyi* and *Operculodinium israelianum* is
227 used here to indicate generally warm, coastal waters. In particular, high percentages of *L.*
228 *machaerophorum* are typically recorded in eutrophic coastal areas where reduced salinity and
229 (seasonal) stratification due to runoff occur (Dale, 1996; Sangiorgi and Donders, 2004;
230 Zonneveld et al., 2009). At present, *T. vancampoeae*, *P. zoharyi* and *O. israelianum* are also
231 found in lagoonal euryhaline environments (Zonneveld et al., 2013), and hence could be used
232 to indicate a more proximal condition relative to *L. machaerophorum* (Pross and Brinkhuis,
233 2005).



234

235 At present, Protoperidinioid (P) cysts are mostly formed by heterotrophic dinoflagellates and
236 the percentage of P cyst may be used as indicator of high eukaryotic productivity (cf. Reichart
237 and Brinkhuis, 2003; Sangiorgi and Donders, 2004). This link has been also extrapolated to
238 the past assemblages (Sluijs et al., 2005). Here we use the percentage of P cysts
239 (*Brigantedinium* spp., *Lejeunecysta* spp., *Trinovantedinium glorianum*, *Dionaeacysta* spp.,
240 *Selenopemphix* spp., *Islandinium* spp., *Barssidinium graminosum*, and *B. wrennii*) to indicate
241 eukaryotic productivity.

242

243 Terrestrial palynomorphs (sporomorphs) reflect variations in the vegetation on the
244 surrounding land masses and provide information on climate variables such as continental
245 temperatures and precipitation (e.g. Heusser and Shackleton, 1979; Donders et al., 2009;
246 Kotthoff et al., 2014). A ratio of terrestrial to marine palynomorphs (T/M ratio) is widely used
247 as a relative measure of distance to the coast and thereby reflects sea level variations and
248 shallowing trends in the basin (e.g. McCarthy and Mudie, 1998; Donders et al., 2009;
249 Quaijtaal et al., 2014; Kotthoff et al., 2014). Morphological characteristics of Late Neogene
250 pollen types can, in most cases, be related to extant genera and families (Donders et al., 2009;
251 Larsson et al., 2011; Kotthoff et al., 2014). In A15-3/4, the relatively long distance to the site
252 of deposition means that the pollen assemblage is not a direct reflection of vegetation cover
253 and climate, but includes information on the mode of transport. Assemblages with a relatively
254 high number of taxa, including insect pollinated forms, are indicative of substantial pollen
255 input through water transport (Whitehead, 1983), whereas wind-transported pollen typically
256 show a low-diversity. Sediments of a location proximal to a river delta likely receive a
257 majority of pollen that is water-transported, while distal locations are dominated by wind-
258 transported pollen and particularly bisaccate taxa (Hooghiemstra, 1988; Mudie and McCarthy,



259 1994). To separate these effects, the percentage of arboreal pollen (AP), representing relative
260 terrestrial temperatures, was calculated excluding bisaccate forms. The non-arboreal pollen
261 (NAP; mainly Poaceae and also *Artemisia*, Chenopodiaceae and Asteraceae) consist only of
262 non-aquatic herbs. High AP percentages indicate warm, moist conditions, whereas open
263 vegetation (NAP and Ericaceae) is indicative for cooler, dryer conditions consistent with a
264 glacial climate.

265

266 *4.3 Palynological processing*

267 The samples were processed using standard palynological procedures (e.g., Faegri et al.,
268 1989) involving HCl (30%) and cold HF (40%) digestion of carbonates and silicates.
269 Residues were sieved with 15 µm mesh and treated by heavy liquid separation (ZnCl₂, specific
270 gravity 2.1 g/cm³). The slides were counted for dinoflagellate cysts, dinocysts (with a
271 minimum of 100 cysts) and pollen (with a preferable minimum of 200 grains). The dinocyst
272 taxonomy is in accordance with that cited in Williams et al. (2017). Resulting counts were
273 expressed as percent abundance of the respective terrestrial or marine groups of
274 palynomorphs.

275

276 *4.4 Organic geochemical proxies*

277 We applied two measures for the relative marine versus terrestrial hydrocarbon
278 sources. The Carbon Preference Index (CPI), based on C₂₅-C₃₄ n-alkanes, originally devised to
279 infer thermal maturity (Bray and Evans, 1961), has high values for predominantly terrestrial
280 plant sources (Rieley et al., 1991). Values closer to one indicate greater input from marine
281 microorganisms and/or recycled organic matter (e.g., Kennicutt et al., 1987). Further, peat
282 mosses like *Sphagnum* are characterized by a dominance of the shorter C₂₃ and C₂₅ n-alkanes,
283 whereas longer chain n-alkanes (C₂₇-C₃₃) are synthesized by higher plants (e.g., Pancost et al.,



284 2002; Nichols et al., 2006), while the C₂₅ n-alkane is characteristic for *Sphagnum* and other
285 mosses in high arctic environments (Vonk and Gustafsson, 2009). Here we express the
286 abundance of *Sphagnum* relative to higher plants as the proportion of C₂₃ and C₂₅ relative to
287 the C₂₇-C₃₃ odd-carbon-numbered n-alkanes. Finally, the input of soil organic matter into the
288 marine environment was estimated using the relative abundance of branched glycerol dialkyl
289 glycerol tetraethers (brGDGTs), primarily produced by soil bacteria, versus that of the marine
290 Thaumarchaeota-derived isoprenoid GDGT crenarchaeol, which is quantified in the Branched
291 and Isoprenoid Tetraether (BIT) index (Hopmans et al., 2004). The relative distribution of
292 brGDGTs in soils is temperature dependent (Weijers et al., 2007; Peterse et al., 2012). Annual
293 mean air temperatures (MAT) were reconstructed based on down-core distributional changes
294 of brGDGT and a global soil calibration that uses both the 5- and 6-methyl isomers of the
295 brGDGTs (MAT_{mr}; De Jonge et al., 2014a). Cyclisation of Branched Tetraethers (CBT)
296 ratios, was shown earlier to correlate with the ambient MAT and soil pH (Weijers et al., 2007;
297 Peterse et al., 2012). The much improved CBT' ratio (De Jonge et al., 2014a), which includes
298 the pH dependent 6-methyl brGDGTs, is used here to represent soil pH. The Total Organic
299 Carbon (TOC) and total nitrogen measurements are used to determine the atomic C/N ratio
300 that in coastal marine sediments indicate the preferential source, with marine C/N values at
301 ~10 and terrestrial between 15 and 30 (Hedges et al., 1997).

302

303 4.5 Organic geochemical processing

304 Organic geochemical analyses were limited to the core and sidewall core samples. For
305 TOC determination For TOC determination ~ 0.3 g of freeze dried and powdered sediment
306 was weighed, and treated with 7.5 ml 1 M HCL to remove carbonates, followed by 4 h
307 shaking, centrifugation and decanting. This procedure was repeated with 12 h shaking.
308 Residues were washed twice with demineralised water dried at 40-50°C for 96 h after which



309 weight loss was determined. ~15 to 20 mg ground sample was measured in a Fisons NA1500
310 NCS elemental analyzer with a normal Dumas combustion setup. Results were normalized to
311 three external standards (BCR, atropine and acetanilide) analyzed before and after the series,
312 and after each ten measurements. % TOC was determined by %C x decalcified
313 weight/original weight.

314

315 For biomarker extraction ca. 10 g of sediment was freeze dried and mechanically powdered.
316 The sediments were extracted with a Dichloromethane (DCM):Methanol (MeOH) solvent
317 mixture (9:1, v/v, 3 times for 5 min each) using an Accelerated Solvent Extractor (ASE,
318 Dionex 200) at 100°C and ca. 1000 psi. The resulting Total Lipid Extract (TLE) was
319 evaporated to near dryness using a rotary evaporator under near vacuum. The TLE then was
320 transferred to a 4 ml vial and dried under a continuous N₂ flow. A 50% split of the TLE was
321 archived. For the working other half elemental sulfur was removed by adding activated (in
322 2M HCl) copper turnings to the TLE in DCM and stirring overnight. The TLE was
323 subsequently filtered over Na₂SO₄ to remove the CuS, after which 500 ng of a C₄₆ GDGT
324 internal standard was added (Huguet et al., 2006). The resulting desulphurized TLE was
325 separated over a small column (Pasteur pipette) packed with activated Al₂O₃ (2 hours h at
326 150°C). The TLE was separated into an apolar, a ketone and a polar fraction by eluting with
327 n-hexane : DCM 9:1 (v/v), n-hexane : DCM 1:1 (v/v) and DCM : MeOH 1:1 (v/v) solvent
328 mixtures, respectively. The apolar fraction was analyzed by gas chromatography (GC)
329 coupled to a flame ionization detector (FID) and gas chromatography/mass spectroscopy
330 (GC/MS) for quantification and identification of specific biomarkers, respectively. For GC,
331 samples were dissolved in 55 µl hexane and analyzed using a Hewlett Packard G1513A
332 autosampler interfaced to a Hewlett Packard 6890 series Gas Chromatography system
333 equipped with flame ionization detection, using a CP-Sil-5 fused silica capillary column (25



334 m x 0.32 mm, film thickness 0.12 μm), with a 0.53 mm pre-column. Temperature program:
335 70°C to 130°C (0 min) at 20°C/min, then to 320°C at 4°C/min (hold time 20 mins).The
336 injection volume of the samples was 1 μl .

337

338 Before GC/MS analyses, 2 μg 5 α -androstane standard was added to the apolar for
339 quantification purposes, assuming a similar ionization efficiency for all components. Analyses
340 were performed on a ThermoFinnigan Trace GC ultra, interfaced to a ThermoFinnigan Trace
341 DSQ MS using the same temperature program, column and injection volume as for GC
342 analysis.

343

344 Prior to analyses, the polar fractions, containing the GDGTs, were dissolved in *n*-hexane :
345 propanol (99:1, v/v) and filtered over a 0.45 μm mesh PTFE filter (\varnothing 4mm). Subsequently,
346 analyses of the GDGTs was performed using ultra high performance liquid chromatography-
347 mass spectrometry (UHPLC-MS) on an Agilent 1290 infinity series instrument coupled to a
348 6130 quadrupole MSD with settings as described in Hopmans et al. (2016). In short,
349 separation of GDGTs was performed on two silica Waters Acquity UHPLC HEB Hilic
350 (1.7 μm , 2.1mm x 150mm) columns, preceded by a guard column of the same material.
351 GDGTs were eluted isocratically using 82% A and 18% B for 25 mins, and then with a linear
352 gradient to 70% A and 30% B for 25 mins, where A is *n*-hexane, and B = *n*-
353 hexane:isopropanol. The flow rate was constant at 0.2 ml/min. The $[\text{M}+\text{H}]^+$ ions of the
354 GDGTs were detected in selected ion monitoring mode, and quantified relative to the peak
355 area of the C₄₆ GDGT internal standard.

356

357 **5 Results**

358 *5.1 Stable isotope data*



359 The *Cassidulina teretis* $\delta^{18}\text{O}$ ($\delta^{18}\text{O}_b$) confirms the relation between glacial stages and fine
360 grained sediment as proposed by Kuhlman et al. (2006a,b), but the data are somewhat
361 scattered (Fig. 3). The glacial-interglacial range in $\delta^{18}\text{O}_b$ is $\sim 1\text{‰}$ between MIS 98 and 97, and
362 $\sim 1.3\text{‰}$ between MIS 95 and 94, but with considerably more variation in especially MIS 95.
363 The $\delta^{13}\text{C}_b$ data vary consistently with the oxygen, and have a glacial-interglacial range of
364 $\sim 1.1\text{‰}$, and one strongly depleted value in MIS 94 (-3.5‰). The $\delta^{13}\text{C}_b$ during MIS 95 are less
365 variable than the $\delta^{18}\text{O}_b$, pointing to an externally forced signal in the latter. The glacial to
366 interglacial ranges are very similar in magnitude with those reported by Sosdian and
367 Rosenthal (2009) for the North Atlantic, but on average lighter by $\sim 0.5\text{‰}$ ($\delta^{18}\text{O}_b$) and $\sim 1.8\text{‰}$
368 ($\delta^{13}\text{C}_b$).

369

370 5.2 Palynology

371 Palynomorphs, including dinocysts, freshwater palynomorphs and pollen, are abundant,
372 diversified, and well-preserved in these sediments. Striking is the dominance by conifer
373 pollen. Angiosperm (tree) pollen are present and diverse, but low in abundance relative to
374 conifers. During interglacials (MIS 103, 99, 97, 95, and 93) the pollen record generally shows
375 increased and more diverse tree pollen (particularly *Picea* and *Tsuga*), and warm temperate
376 *Osmunda* spores, whereas during glacials (MIS 102, (100), 98, 96, and 94) herb and heath
377 pollen indicative of open landscapes are dominant (Fig S2). The % arboreal pollen (AP)
378 summarizes these changes, showing maximum values of $>40\%$ restricted to just a part of the
379 coarser grained interglacial intervals (Fig. 3). The percentage record of cold-loving dinocysts
380 is quite scattered in some intervals but indicates generally colder conditions within glacial
381 stages, and minima during %AP maxima (Fig. 3). After peak cold conditions and a TOC
382 maximum (see below), but still well within the glacials, the % Protoperidinoid consistently
383 increases. Some intervals (e.g., top of MIS 94) are marked by influxes of freshwater algae,



384 indicating a strong riverine input, these data however do not indicate a clear trend. This robust
385 in-phase pattern of glacial-interglacial variations is also reflected by high T/M ratios during
386 glacials, indicating coastal proximity, and low T/M during (final phases of) interglacials. The
387 Glacial-Interglacial (G-IG) variability in the T/M ratio is superimposed on a long-term
388 shoaling trend of the marine environment. The coastal (warm-tolerant) dinocyst maxima are
389 confined to the interglacial intervals and their abundance increases throughout the record.
390 Successive increases of coastal inner neritic *Lingulodinium machaerophorum*, followed by
391 increases in coastal lagoonal species in the youngest part, mirror the shoaling trend in the T/M
392 ratio, which reflect the gradual progradation of the Eridanos delta front (Fig. S1).

393

394 5.3 Organic geochemical proxies

395 Lowest TOC weight % values are reached in the clay intervals, and typically range between
396 0.5% in glacials and 1% in interglacials (Fig. 3). Nitrogen concentrations are relatively stable
397 resulting in C/N ratios primarily determined by carbon content, ranging between ~8-9
398 (glacials) and ~14 and 17 (interglacials). The Carbon Preference Index (CPI) is generally
399 high, reflecting a continuous input of immature terrestrial organic matter. Minimum CPI
400 values of ~2.8 - 2.9 are reached at the transitions from the coarser sediments to the clay
401 intervals after which they increase to maxima of 4.5 - 5.0 in the late interglacials. The *n*-C₂₃
402 *Sphagnum* biomarker correlates consistently with the T/M ratio, %AP, and cold water
403 dinocysts, while the variation in the CPI index is partially out of phase; it is more gradual and
404 lags the % TOC and other signals. Generally lower Branched and Isoprenoid Tetraether (BIT)
405 values during interglacials indicate more marine conditions, i.e. larger distance to the coast
406 and relatively reduced terrestrial input from the Eridanos catchment (cf. Sinninghe Damsté,
407 2016). As both brGDGT input (run off, soil exposure and erosion) and sea level (distance to
408 the coast) vary across G-IG timescales, for example during deglaciation and subsequent



409 reactivation of fluvial transport (Bogaart and van Balen, 2000), the variability of the BIT
410 index is somewhat different compared to the T/M palynomorph ratio, but is generally in phase
411 with gradual transitions along G-IG cycles. The MAT_{mr}-based temperature reconstructions
412 vary between 5 and 17°C, reaching maximum values in MIS 97. However, in the MIS 99/98
413 and MIS96/95 transitions the MAT_{mr} shows variability opposite to the identified G-IG cycles
414 and the signal contains much high-order variability. Low values during interglacials coincide
415 with low reconstructed soil pH (CBT-pH).

416

417 *Figure 3: spliced record of A15-3 and A15-4 showing the principal organic geochemical and*
418 *palynological indices. Shaded blue intervals represent the identified glacial MIS delimited by*
419 *the gamma-ray transitions following Kuhlmann et al. (2006a,b). Data density is dependent on*
420 *type of sample as indicated in Fig. 1. Age scale is based on correlation and LOESS*
421 *interpolation of the identified MIS transitions to the LR04 benthic stack (Lisiecki and Raymo,*
422 *2005) as shown in Fig S3. Data is available in Tables S and 2.*

423



427 **6 Discussion**

428 *6.1 Paleoenvironmental setting*

429 During MIS 103, 99, 97, 95, and 93 the pollen record indicates generally warmer and more
430 humid conditions than during MIS 102, 98, 96, and 94 (Fig. 3). The cold-water temperature
431 signal based on dinocysts is more variable than the terrestrial cooling as derived from pollen.
432 Pollen represents mean standing vegetation in the catchment, and also depends on dominant
433 circulation patterns and short-term climate variations (Donders et al., 2009). Due to exclusion
434 of bisaccate pollen, the %AP is generally low. However, in this way we excluded the climate
435 signal bias due to direct effect of sea level changes (Donders et al., 2009; Kotthoff et al.,
436 2014). Given the average sample distance, on a glacial-interglacial time scale no significant
437 phase differences between the terrestrial and the marine signal appear. In the record there are
438 small time lags between proxies, which have important implications for explaining the forcing
439 of G-IG cycles and will further be explained in more detail. In the best constrained MIS
440 transition (98 to 97), the G-IG transition is seen first in decreases of the cold water dinocysts
441 and $n\text{-C}_{23+25}$ *Sphagnum* biomarkers, subsequently the BIT decrease, MAT and the %AP
442 increases, and finally in the $\delta^{18}\text{O}_b$ and T/M ratio decreases that lag by a few thousand years
443 (Fig. 3). The CPI signal is more gradual, but generally in line with T/M. The high variability
444 and strongly depleted values in $\delta^{18}\text{O}_b$ during MIS 95 occur during peak coastal dinocyst
445 abundances, suggesting high run off phases during maximum warming. During cold water
446 dinocysts maxima, the high abundance of Protoperidinioids indicates high nutrient input, and
447 productive spring/summer blooms, which point to strong seasonal temperature variations.
448 This productivity signal markedly weakens in MIS 94 and 92 and the gradual T/M increase is
449 consistent with the basin infill and gradually approaching shelf-edge delta (Fig. S1). As
450 Protoperidinioid minima generally occur during TOC maxima there is no indication for a
451 preservation overprint of the P-cysts. Combined, the high TOC and CPI values, coastal and



452 stratified water conditions, and intervals of depleted $\delta^{18}\text{O}_b$ document increased Eridanos run-
453 off during interglacials. These suggest a primarily terrestrial organic matter source that, based
454 on mineral provenance studies (Kuhlmann et al., 2004) and high conifer pollen abundance
455 documented here, likely originated from the Fennoscandian Shield. The fine-grained material
456 during cold phases is probably transported by meltwater during summer from local glaciers
457 that developed since the Late Pliocene at the surrounding Scandinavian mainland (Mangerud
458 et al., 1996; Kuhlmann et al., 2004).

459

460 Whereas the BIT index reflects the G-IG cycles, the MAT_{mr} record, which is also based on
461 brGDGTs, has a variable phase relation with the G-IG cycles and high variability. The use of
462 MAT_{mr} in coastal marine sediments is based on the assumption that river-deposited brGDGTs
463 reflect an integrated signal of the catchment area. As the Eridanos system is reactivated
464 following glacials, glacial soils containing brGDGT are likely eroded causing a mixed signal
465 of glacial and interglacial material. The lowest MAT_{mr} and highest variability is indeed
466 observed during high TOC input and minima of CBT'-pH below 6 (Fig. 3), consistent with
467 increased erosion of acidic glacial (peat) soil. This suggests that the variability in the MAT_{mr}
468 record is not fully reliable. Alternatively, the terrestrial brGDGT signal may be altered by a
469 contribution of brGDGTs produced in the marine realm. BrGDGTs were initially believed to
470 be solely produced in soils, but emerging evidence suggests that brGDGTs are also produced
471 during river transport (e.g., Zell et al., 2013; De Jonge et al., 2014b) and in the coastal marine
472 environment (e.g., Peterse et al., 2009; Sinninghe Damsté, 2016), which, points to significant
473 terrestrial contributions in our record. Based on the modern system, the degree of cyclisation
474 of tetramethylated brGDGTs ($\#rings_{\text{tetra}}$) has been proposed to identify a possible in situ
475 overprint (Sinninghe Damsté, 2016). However, the $\#rings_{\text{tetra}}$ in this sediment core is <0.37 ,
476 which is well below the suggested threshold of 0.7, and thus suggests that the brGDGTs are



477 primarily soil-derived. Finally, selective preservation in the catchment and during fluvial
478 transport may have affected the brGDGT signal, although experimental evidence on fluvial
479 transport processes indicates that these do not significantly affect initial soil-brGDGT
480 compositions (Peterse et al., 2015). The T/M ratio variability corresponds well to the LR04
481 benthic stack (Fig. 3), which is primarily an obliquity signal. Within the constraints of the
482 sample availability, our record captures the approximate symmetry between glaciation and
483 deglaciation typical of the Early Pleistocene (Lisiecki and Raymo, 2005).

484

485 *6.2 Implications for the onset of Northern Hemisphere glaciations*

486 The classic Milankovitch model predicts that global ice volume is forced by high northern
487 summer insolation (e.g. Hays et al., 1976). Raymo et al. (2006) suggested an opposite
488 response of ice sheets on both hemispheres due to precession forcing, cancelling out the signal
489 and amplifying obliquity in the Early Pleistocene. That suggestion predicts that regional
490 climate records on both hemispheres should contain a precession component that is not visible
491 in the sea level and deep sea $\delta^{18}\text{O}_b$ record. Our results show that the regional NH climate on
492 both land and sea surface varies in concert with local relative sea level which, with the best
493 possible age information so far, is consistent with the LR04 $\delta^{18}\text{O}_b$ record. Contrary to the
494 model proposed by Raymo et al. (2006), this suggests that the NH obliquity forcing is the
495 primary driver for the glacial-interglacial in the Early Pleistocene. The small lead of the
496 temperature proxies over the local sea level further supports the NH obliquity forcing scenario
497 as cooling would precede ice buildup. Various studies indicate the importance of gradual CO_2
498 decline in the intensification of NHG (Kürschner et al., 1996; Seki et al., 2010; Bartoli et al.,
499 2011) combined with the threshold effects of ice albedo (Lawrence et al., 2010; Etourneau et
500 al., 2010) and land cover changes (Koenig et al., 2011). Simulations of four coupled 3-D ice



501 models indicate that Antarctic ice volume increase responds primarily to sea level lowering,
502 while Eurasian and North American ice sheet growth is initiated by temperature decrease (De
503 Boer et al., 2012). The latter dominate the eustatic sea level variations during glacials. Our
504 observations agree with the modelled temperature sensitivity of NH ice sheet growth. The
505 dominant obliquity signal further suggests a seasonal aspect of the climate forcing. The
506 combination of high summer productivity, based on increased Protoperidinioid dinocysts, and
507 increased proportions of cold dinocysts during the glacials in the SNS record indicate a strong
508 seasonal cycle. This confirms similar results from the North Atlantic (Hennissen et al., 2015)
509 and is consistent with an obliquity-driven glacial-interglacial signal in a mid-latitude
510 setting, likely promoting meridional humidity transport and ice buildup.

511

512 The southward migration of Arctic surface water masses indicated by increases in cold water
513 dinocysts (Fig. 3) is furthermore relevant for understanding the relation between the Atlantic
514 meridional overturning circulation (AMOC) intensity and ice sheet growth (e.g. Bartoli et al.,
515 2005; Naafs et al, 2010). Mid Pliocene increased heat transport and subsequent decrease
516 during NHG due to AMOC intensity changes has been invoked from many proxy records but
517 is difficult to sustain in models (Zhang et al., 2013). Our results indicate that the NW
518 European Early Pleistocene climate experienced severe cooling during sea level lowstands,
519 which is consistent with southward displacement of the Arctic front and decreased AMOC
520 (Naafs et al., 2010). The data-model mismatch in AMOC changes might be due to dynamic
521 feedbacks in vegetation or (sea-) ice (Koenig et al., 2011; de Boer et al., 2012) that are
522 prescribed variables in the model comparison by Zhang et al. (2013).

523



524 Our SNS record provides a well-dated Early Pleistocene Glacial-Interglacial succession
525 integrating marine and terrestrial signals improving on the classic terrestrial Praetiglian stage.
526 While conceptually valid, the earliest Pleistocene glacial stages defined in the continental
527 succession of the SE Netherlands (Van der Vlerk and Florschütz, 1953; Zagwijn, 1960) and
528 currently considered text book knowledge, are highly incomplete and locally varied (Donders
529 et al., 2007). This shallow marine SNS record provides a much more suitable reflection of
530 large-scale transitions and trends in NW Europe and merits further development by complete
531 recovery of the sequence in a scientific drilling project (Westerhoff et al, 2016).

532

533 **7 Conclusions**

534 The independently dated Late Pliocene-Early Pleistocene sedimentary succession of the
535 southern North Sea Basin provides a record that straddles the onset of Northern Hemisphere
536 Glaciation and the subsequent climate fluctuations in a shallow marine setting in great detail.
537 The onset of the glaciation and the correlation to marine isotope stages 103 to 92, including
538 the conspicuous stages 100, 98 to 96 representing the first cold Pleistocene stages, is well
539 expressed in the marine and terrestrial palynomorph and organic biomarker records of the
540 southern North Sea. The independent relative sea- and land-based temperature records show
541 clearly coeval (at this resolution) cold and warm glacial-interglacial and sea level cycles that
542 are well-correlated to the LR04 benthic stack. Critically, both the biomarker signals, %AP,
543 and cold water dinocyst variations show consistent in-phase variability on obliquity time
544 scales, leading sea level changes, which supports a dominantly direct NH insolation control
545 over Early Pleistocene glaciations. Based on this integrated record, NH obliquity forcing is
546 the primary driver for the glacial-interglacial in the Early Pleistocene. Furthermore, our
547 findings support the theory of temperature sensitivity of NH ice sheet growth. The



548 interglacials are characterized by (seasonally) stratified waters and/or near-shore conditions as
549 glacial-interglacial cycles became more expressive and the Eridanos delta progressed into the
550 region. The strong seasonality at mid-latitudes point to a vigorous hydrological cycling that
551 should be considered as a potential factor in ice sheet formation in further investigations.

552

553 **8 Author contributions**

554 THD, HB and GK designed the research. NvH carried out the geochemical analyses under
555 supervision from GJR, JSD, JW and FP. RV, DM and THD carried out the palynological
556 analyses and interpreted the data together with FS. LL and RPS provided stable isotope data
557 on benthic foraminifera. JtV provided seismic interpretations. THD integrated the data wrote
558 the paper with contributions from all authors.

559

560 **9 Acknowledgements**

561 We gratefully acknowledge the support in providing the offshore samples to this study and
562 permission to publish by Wintershall Noordzee B.V., and project support by partners Chevron
563 Exploration and Production Netherlands B.V., Total E&P Nederland B.V., Dana Petroleum
564 Netherlands B.V., Oranje-Nassau Energie B.V., and Energie Beheer Nederland (EBN).
565 Arnold van Dijk is thanked for running C/N and stable isotope analyses, and Giovanni
566 Dammers for processing palynological samples.

567

568 **10 References**

569 Bakken, K. and Dale, B., 1986. Dinoflagellate cysts in Upper Quaternary sediments from
570 southwestern Norway and potential correlations with the oceanic record: *Boreas* 15: 185-190.



- 571 Bartoli, G., Hoenisch, B., Zeebe, R.E., 2011. Atmospheric CO₂ decline during the Pliocene
572 intensification of Northern Hemisphere glaciations. *Paleoceanography* 26, PA4213.
573 <http://dx.doi.org/10.1029/2010PA002055>.
- 574 Bijlsma, S., 1981. Fluvial sedimentation from the Fennoscandian area into the Northwest
575 European Basin during the Late Cenozoic. *Geologie en Mijnbouw* 60: 337-345.
- 576 Bogaart, P.W., Van Balen, R.T., 2000. Numerical modeling of the response of alluvial rivers
577 to Quaternary climate change. *Global and Planetary Change* 27: 147-163.
- 578 Bray, E.E., and Evans, E.D., 1961. Distribution of n-paraffins as a clue to recognition of
579 source beds, *Geochimica et Cosmochimica Acta* 22: 2-15.
- 580 Brierley, C.M., and Fedorov, A.V., 2010. Relative importance of meridional and zonal sea
581 surface temperature gradients for the onset of the ice ages and Pliocene - Pleistocene climate
582 evolution. *Paleoceanography* 25: PA2214, doi:10.1029/2009PA001809.
- 583 Brigham-Grette, J, Melles, M., Minyuk, P.S., Andreev, A.A., Tarasov, P.E., DeConto, R.M.,
584 König, S. Nowaczyk, N.R., Wennrich, V., Rosén, P., Haltia-Hovi, E., Cook, T.L., Gebhardt,
585 C., Meyer-Jacob, C., Snyder, J.A., Herzschuh, U., 2013. Pliocene warmth, polar
586 amplification, and stepped Pleistocene cooling recorded in NE Arctic Russia. *Science* 340:
587 1421-1427.
- 588 Caston, V.N.D., 1979. The Quaternary sediments of the North Sea. In: Banner, F.T., Collins,
589 M.B., Massie, K.S. (Eds.), *The north-west European shelf seas: the sea bed and the sea in
590 motion. I. Geology and Sedimentology*, Elsevier Oceanographic Series 24A, p. 195-270.
- 591 Dale, B., 1996. Dinoflagellate cyst ecology: modelling and geological applications. In: J.M.G.
592 Jansonius, D.C. (Editor), *Palynology: Principles and Application*, vol. 3. American
593 Association of Stratigraphic Palynologists Foundation, College Station, TX: 1249-1275.
- 594 de Boer, B., van de Wal, R.S.W., Lourens, L.J., Bintanja, R., Reerink, T.J., 2012. A
595 continuous simulation of global ice volume over the past 1 million years with 3-D ice-sheet
596 models. *Climate Dynamics* 41, 1365. doi:10.1007/s00382-012-1562-2
- 597 De Haas, H., Boer, W., van Weering, T.C.E., 1997. Recent sediment and organic carbon
598 burial in a shelf sea; the North Sea. *Marine Geology* 144, 131–146.
- 599 De Jonge, C., Hopmans, A.C, Zell, C.I., Kim, J.-H., Schouten, S., Sinninghe Damsté, J.S.,
600 2014a. Occurrence and abundance of 6-methyl branched glycerol dialkyl glycerol tetraethers
601 in soils: Implications for palaeoclimate reconstruction. *Geochimica et Cosmochimica Acta*
602 141: 97-112.
- 603 De Jonge, C., Stadnitskaia, A., Hopmans, E.C., Cherkashov, G., Fedotov, A. and Sinninghe
604 Damsté, J.S., 2014b. In-situ produced branched glycerol dialkyl glycerol tetraethers in
605 suspended particulate matter from the Yenisei River, Eastern Siberia. *Geochimica et
606 Cosmochimica Acta* 125, 476–491.



- 607 De Schepper, S., Head, M.J., and Louwye, S., 2009. Pliocene dinoflagellate cyst stratigraphy,
608 palaeoecology and sequence stratigraphy of the Tunnel-Canal Dock, Belgium, Geological
609 Magazine 146, 92 - 112, doi: 10.1017/S0016756808005438.
- 610 De Schepper, S., Fischer, E.I., Groeneveld, J., Head, M.J., Matthiessen, J., 2011. Deciphering
611 the palaeoecology of Late Pliocene and Early Pleistocene dinoflagellate cysts.
612 Palaeogeography, Palaeoclimatology, Palaeoecology 309: 17–32.
- 613 De Schepper, S., Groeneveld, J., Naafs, B.D.A., Van Renterghem, C., Hennissen, J., Head,
614 M.J., Louwye, S., Fabian, K., 2013. Northern Hemisphere glaciation during the globally
615 warm early Late Pliocene. PLoS ONE 8 (12), e81508.
616 <http://dx.doi.org/10.1371/journal.pone.0081508>.
- 617 De Vernal, A., 2009. Marine palynology and its use for studying nearshore environments,
618 From Deep-Sea to Coastal Zones: Methods – Techniques for Studying Paleoenvironments,
619 IOP Conference Series: Earth and Environmental Science, 5, 012002, doi:10.1088/1755-
620 1307/5/1/012002.
- 621 Donders, T.H., Kloosterboer-van Hoeve, M.L., Westerhoff, W., Verreussel, R.H.C.M. &
622 Lotter, A.F., 2007. Late Neogene continental stages in NW Europe revisited. Earth-Science
623 Reviews 85: 161-186.
- 624 Donders, T.H., Weijers, J.W.H., Munsterman, D.K., Kloosterboer-van Hoeve, M.L., Buckles,
625 L.K., Pancrost, R.D., Schouten, S., Sinninghe Damsté, J.S. & Brinkhuis, H., 2009. Strong
626 climate coupling of terrestrial and marine environments in the Miocene of northwest Europe.
627 Earth and Planetary Science Letters 281 (3-4): 215-225.
- 628 Etourneau, J., Schneider, R., Blanz, T., Martinez, P., 2010. Intensification of the Walker and
629 Hadley atmospheric circulations during the Pliocene-Pleistocene climate transition. Earth and
630 Planetary Science Letters 297: 103-110. <http://dx.doi.org/10.1016/j.epsl.2010.06.010>.
- 631 Faegri, K., Iversen, J., Kaland, P.E., Krzywinski, K., 1989, Text book of pollen analysis, IV
632 Edition. The Blackburn Press, 328 pp.
- 633 Head, M.J., 1996. Modern dinoflagellate cysts and their biological affinities. In: Jansonius, J.,
634 McGregor, D.C. (Eds.), Palynology: Principles and Application, vol. 3. American Association
635 of Stratigraphic Palynologists Foundation, College Station, TX, pp. 1197-1248.
- 636 Haug, G.H. and Tiedemann, R., 1998. Effect of the formation of the Isthmus of Panama on
637 Atlantic Ocean thermohaline circulation: Nature 393 (6686): 673- 676.
- 638 Haug, G.H., Sigman, D.M., Tiedemann, R., Pedersen, T.F. & Sarnthein, M., 1999. Onset of
639 permanent stratification in the subarctic Pacific Ocean. Nature 40: 779–782.
- 640 Haug, G.H., Ganopolski, A., Sigman, D.M., Rosell-Mele, A., Swann, G. E. A, Tiedemann, R.,
641 Jaccard, S. L., Bollmann, J., Maslin, M.A., Leng, M.J. and G. Eglinton, 2005. North Pacific
642 seasonality and the glaciation of North America 2.7 million years ago: Nature 433: 821-825.



- 643 Hays, J. D., Imbrie, J. & Shackleton, N. J., 1976. Variations in the Earth's orbit: pacemaker of
644 the ice ages. *Science* 194; 1121–1132.
- 645 Head, M.J., Riding, J.B., Eidvin, T., Chadwick, R.A., 2004. Palynological and foraminiferal
646 biostratigraphy of (Upper Pliocene) Nordland Group mudstones at Sleipner, northern North
647 Sea. *Marine and Petroleum Geology* 21:277-297.
648 <http://dx.doi.org/10.1016/j.marpetgeo.2003.12.002>.
- 649 Hedges, J.I., Keil, R.G., & Benner, R., 1997. What happens to terrestrial organic matter in the
650 ocean? *Organic geochemistry* 27: 195-212.
- 651 Hennissen, J.A.I., Head, M.J., De Schepper, S., Groeneveld, J., 2015. Increased seasonality
652 during the intensification of Northern Hemisphere glaciation at the Pliocene-Pleistocene
653 transition ~2.6 Ma. *Quaternary Science Reviews* 129, 321–332.
- 654 Hennissen, J.A.I., Head, M.J., De Schepper, S., Groeneveld, J., 2017. Dinoflagellate cyst
655 paleoecology during the Pliocene–Pleistocene climatic transition in the North Atlantic,
656 *Palaeogeography, Palaeoclimatology, Palaeoecology* 470: 81-108.
- 657 Heusser, L.E., and Shackleton, N.J., 1979. Direct marine-continental correlation: 150,000-
658 year oxygen isotope-pollen record from the North Pacific. *Science* 204: 837-839.
- 659 Hooghiemstra, H., 1988. Palynological records from Northwest African marine sediments: a
660 general outline of the interpretation of the pollen signal. *Philosophical Transactions of the*
661 *Royal Society of London, Series B Biological Sciences* 318 (1191): 431–449.
- 662 Hooghiemstra, H., Ran, E.T.H., 1994. Late Pliocene-Pleistocene high resolution pollen
663 sequence of Colombia: An overview of climatic change. *Quaternary International*, 21: 63-80
- 664 Hopmans, E.C., Weijers, J.W.H., Schefuss, E., Herfort, L., Sinninghe Damsté, J.S., Schouten,
665 S., 2004. A novel proxy for terrestrial organic matter in sediments based on branched and
666 isoprenoid tetraether lipids. *Earth and Planetary Science Letters* 24: 107–116.
- 667 Hopmans, E.C., Schouten, S., Sinninghe Damsté, J.S., 2016. The effect of improved
668 chromatography on GDGT-based palaeoproxies. *Organic Geochemistry* 93: 1-6.
- 669 Huuse, M., Lykke-Andersen, H., Michelsen, O., 2001, Cenozoic evolution of the eastern
670 North Sea Basin – new evidence from high-resolution and conventional seismic data: *Marine*
671 *Geology* 177: 243-269.
- 672 Huybers, P., 2011. Combined obliquity and precession pacing of late Pleistocene
673 deglaciations. *Nature* 480: 229–232, doi:10.1038/nature10626.
- 674 Keigwin, L. D., 1982. Isotope paleoceanography of the Caribbean and east Pacific: role of
675 Panama uplift in late Neogene time. *Science* 217: 350–353.
- 676 Kemna, H.A., Westerhoff, W.E., 2007. Remarks on the palynology-based chronostratigraphic
677 subdivision of the Pliocene terrestrial deposits in NW-Europe. *Quaternary International* 164–
678 165: 184–196.



- 679 Kennicutt II, M.C., Barker, C., Brooks, J.M., DeFreitas, D.A., Zhu, G.H., 1987. Selected
680 organic matter source indicators in the Orinoco, Nile and Changjiang deltas. *Organic*
681 *Geochemistry* 11, 41-51.
- 682 Knies, J., Cabedo-Sanz, P., Belt, S.T., Baranwal, S., Fietz, S., Rosell-Mele, A., 2014. The
683 emergence of modern sea ice cover in the Arctic Ocean. *Nature Communications* 5:
684 <http://dx.doi.org/10.1038/ncomms6608>.
- 685 Koenig, S.J., DeConto, R.M. & Pollard, D., 2011. Late Pliocene to Pleistocene sensitivity of
686 the Greenland Ice Sheet in response to external forcing and internal feedbacks. *Climate*
687 *Dynamics* 37: 1247. doi:10.1007/s00382-011-1050-0.
- 688 Kotthoff, U., Greenwood, D., McCarthy, F., Müller-Navarra, K., Prader, S., Hesselbo, S.,
689 2014. Late Eocene to middle Miocene (33 to 13 million years ago) vegetation and climate
690 development on the North American Atlantic Coastal Plain (IODP Expedition 313, Site
691 M0027). *Climate of the Past* 10: 1523-1539.
- 692 Kuhlmann, G. & Wong, T.E., 2008. Pliocene paleoenvironment evolution as interpreted
693 from 3D-seismic data in the southern North Sea, Dutch offshore sector. *Marine and Petroleum*
694 *Geology* 25: 173-189.
- 695 Kuhlmann, G., Pedersen, R.-B., de Boer, P., Wong, Th.E., 2004. Provenance of Pliocene
696 sediments and paleoenvironmental change in the southern North Sea region using Sm/Nd
697 (samarium-neodymium) provenance ages and clay mineralogy. *Sedimentary Geology* 171:
698 205-226.
- 699 Kuhlmann, G., Langereis, C.G., Munsterman, D., van Leeuwen, R.-J., Verreussel, R.,
700 Meulenkamp, J., Wong, Th.E., 2006a. Chronostratigraphy of Late Neogene sediments in the
701 southern North Sea Basin and paleoenvironmental interpretations. *Palaeogeography,*
702 *Palaeoclimatology, Palaeoecology* 239: 426-455.
- 703 Kuhlmann, G., Langereis, C.G., Munsterman, D., van Leeuwen, R.-J., Verreussel, R.,
704 Meulenkamp, J.E., Wong, Th.E., 2006b. Integrated chronostratigraphy of the Pliocene-
705 Pleistocene interval and its relation to the regional stratigraphical stages in the southern North
706 Sea region. *Netherlands Journal of Geosciences - Geologie en Mijnbouw* 85 (1): 19-35.
- 707 Kürschner, W.A., Van Der Burgh, J., Visscher, H., and Dilcher, D.L., 1996. Oak leaves as
708 biosensors of late Neogene and early Pleistocene paleoatmospheric CO₂ concentrations.
709 *Marine Micropaleontology* 27: 299-312.
- 710 Larsson, L.M., Dybkjaer, K., Rasmussen, E.S., Piasecki, S., Utescher, T., and Vajda, V.,
711 2011. Miocene climate evolution of northern Europe: A palynological investigation from
712 Denmark. *Palaeogeography, Palaeoclimatology, Palaeoecology* 309: 161-175.
- 713 Lawrence, K.T., Sosdian, S., White, H.E., Rosenthal, Y., 2010. North Atlantic climate
714 evolution through the Plio-Pleistocene climate transitions, *Earth and Planetary Science Letters*
715 300: 329-342, <http://dx.doi.org/10.1016/j.epsl.2010.10.013>.



- 716 Lisiecki, L.E., and Raymo, M.E., 2005. A Pliocene-Pleistocene stack of 57 globally
717 distributed benthic $\delta^{18}\text{O}$ records. *Paleoceanography* 20: PA1003, doi:10.1029/2004PA001071.
- 718 Lister, A.M., 2004. The impact of Quaternary Ice Ages on mammalian evolution.
719 *Philosophical Transactions of the Royal Society of London, Series B Biological Sciences* 359,
720 221-241.
- 721 Mackensen, A. & Hald, M., 1988. *Cassidulina teretis* Tappan and *C. laevigata* d'Orbigny:
722 their modern and late Quaternary distribution in northern seas. *Journal of Foraminiferal*
723 *Research* 18 (1): 16-24.
- 724 Mangerud, J., Jansen, E., Landvik, J., 1996. Late Cenozoic history of the Scandinavian and
725 Barents Sea ice sheets: *Global and Planetary Change* 12, 11-26.
- 726 Maslin, M.A., Li, X. S., Loutre M. F., & Berger A. 1998. The contribution of orbital forcing
727 to the progressive intensification of Northern Hemisphere Glaciation. *Quaternary Science*
728 *Reviews*, 17, 411-426.
- 729 McCarthy, F.M.G. and Mudie, P., 1998. Oceanic pollen transport and pollen:dinocyst ratios
730 as markers of late Cenozoic sea level change and sediment transport. *Palaeogeography,*
731 *Palaeoclimatology, Palaeoecology* 138: 187-206.
- 732 Meijer, T., Cleveringa, P., Munsterman, D. K. and Verreussel, R. M. C. H. 2006. The Early
733 Pleistocene Praetiglian and Ludhamian pollen stages in the North Sea Basin and their
734 relationship to the marine isotope record. *Journal of Quaternary Science* 21: 307–310.
- 735 Meloro, C., Raia, P., Carotenuto, F., Barbera, C., 2008. Diversity and turnover of Plio-
736 Pleistocene large mammal fauna from the Italian Peninsula, *Palaeogeography,*
737 *Palaeoclimatology, Palaeoecology* 268, 58-64.
- 738 Michelsen, O., Thomsen, E., Danielsen, M., Heilmann-Clausen, C., Jordt, H., Laursen, G-V.,
739 1998. Cenozoic sequence stratigraphy in eastern North Sea. In: P.-C. de Graciansky, T.
740 Jacquin, P.R. Vail and M.B. Farley (Eds), *Mesozoic and Cenozoic sequence stratigraphy of*
741 *European Basins: SEPM (Society for Sedimentary Geology) Special Publications* 60, 91-118.
- 742 Mudelsee, M. and Raymo, M.E., 2005. Slow dynamics of the Northern Hemisphere
743 glaciation. *Paleoceanography* 20, PA4022.
- 744 Mudie, P.J. and McCarthy, F.M.G., 1984. Late Quaternary pollen transport processes, western
745 North Atlantic: Data from box models, cross-margin and N-S transects. *Marine Geology*, 118:
746 79-105.
- 747 Naafs, B.D.A., Stein, R., Hefter, J., Khelifi, N., De Schepper, S., Haug, G.H., 2010. Late
748 Pliocene changes in the North Atlantic current. *Earth and Planetary Science Letters* 298: 434-
749 442. <http://dx.doi.org/10.1016/j.epsl.2010.08.023>.



- 750 Nichols, J.E., Booth, R.K., Jackson, S.T., Pendall, E.G. & Huang, Y., 2006. Paleohydrologic
751 reconstruction based on n-alkane distributions in ombrotrophic peat. *Organic Geochemistry*
752 37: 1505-13.
- 753 Overeem, I., G. J. Weltje, C. Bishop-Kay and S. B. Kroonenberg, 2001, The Late Cenozoic
754 Eridanos delta system in the Southern North Sea Basin: a climate signal in sediment supply?:
755 *Basin Research* 13: 293-312.
- 756 Pagani, M., Liu, Z., LaRiviere, J., Ravelo, A.C., 2010. High Earth-system climate sensitivity
757 determined from Pliocene carbon dioxide concentrations. *Nature Geoscience*. 3: 27-30.
758 <http://dx.doi.org/10.1038/NGEO724>.
- 759 Pancost, R.D., Baas, M., van Geel, B., & Damsté, J.S.S., 2002. Biomarkers as proxies for
760 plant inputs to peats: an example from a sub-boreal ombrotrophic bog. *Organic Geochemistry*,
761 33(7): 675-690.
- 762 Peterse, F., Moy, C.M., and Eglinton, T.I., 2015. A laboratory experiment on the behaviour of
763 soil-derived core and intact polar GDGTs in aquatic environments. *Biogeosciences* 12: 933–
764 943, doi:10.5194/bg-12-933-2015.
- 765 Peterse, F., Kim, J.-H., Schouten, S., Kristensen, D.K., Koç, N. & Sinninghe Damsté, J.S.
766 2009. Constraints on the application of the MBT/CBT palaeothermometer at high latitude
767 environments (Svalbard, Norway). *Organic Geochemistry*. 40 (6): 692-699
- 768 Poore, H.R., Samworth, R., White, N.J., Jones, S.M., McCave, I.N., 2006. Neogene overflow
769 of Northern Component Water at the Greenland–Scotland Ridge. *Geochemistry Geophysics*
770 *Geosystems* 7. <http://dx.doi.org/10.1029/2005gc001085.Q06010>.
- 771 Pross, J. and Brinkhuis, H., 2005. Organic-walled dinoflagellate cysts as paleoenvironmental
772 indicators in the Paleogene; a synopsis of concepts. *Paläontologische Zeitschrift*, 79(1): 53-
773 59.
- 774 Reichart, G.J. and Brinkhuis, H., 2003. Late Quaternary *Protoperidinium* cysts as indicators of
775 paleoproductivity in the northern Arabian Sea: *Marine Micropaleontology* 49: 303-315.
- 776 Rosoff, D.B., and Corliss, B.H., 1992. An analysis of Recent deep-sea benthic foraminiferal
777 morphotypes from the Norwegian and Greenland seas. *Palaeogeography, Palaeoclimatology,*
778 *Palaeoecology* 91, 13-20.
- 779 Quaijtaal, W., Donders, T.H., Persico, D. & Louwye, S., 2014. Characterising the middle
780 Miocene Mi-events in the Eastern North Atlantic realm - A first high-resolution marine
781 palynological record from the Porcupine Basin. *Palaeogeography, Palaeoclimatology,*
782 *Palaeoecology* 399: 140-159.
- 783 Ravelo, A.C., Andreasen, D.H., Lyle, M., Lyle, A.O., Wara, M.W., 2004. Regional climate
784 shifts caused by gradual global cooling in the Pliocene epoch. *Nature* 429 (6989): 263-267.
- 785 Ravelo, A.C., 2010. Palaeoclimate: Warmth and glaciation. *Nature Geoscience* 3: 672–674



- 786 Raymo, M.E., 1994. The initiation of Northern Hemisphere glaciation. *Annual Review of*
787 *Earth and Planetary Sciences* 22, 353-383.
788 <http://dx.doi.org/10.1146/annurev.earth.22.050194.002033>.
- 789 Raymo, M.E., Ruddiman, W.F., Backman, J., Clement, B. M., and Martinson, D.G., 1989.
790 Late Pliocene variation in Northern Hemisphere ice sheets and North Atlantic Deep Water
791 circulation, *Paleoceanography* 4: 413–446.
- 792 Raymo, M. E., Lisiecki, L. & Nisancioglu, K.. 2006. Plio–Pleistocene ice volume, Antarctic
793 climate, and the global $\delta^{18}\text{O}$ record. *Science* 313: 492–495.
- 794 Reichart, G.J., Brinkhuis, H., 2003. Late Quaternary *Protoperidinium* cysts as indicators of
795 paleoproductivity in the northern Arabian Sea. *Marine Micropaleontology* 49 : 303-315.
- 796 Rieley, G., Collier, R.J., Jones, D.M., Eglinton, G., 1991. The biogeochemistry of Ellesmere
797 Lake, U.K. I: source correlation of leaf wax inputs to the sedimentary lipid record. *Organic*
798 *Geochemistry* 17: 901–912.
- 799 Rochon, A., de Vernal, A., Turon, J.L., Mathiessen, J., Head, M.J., 1999. Distribution of
800 recent dinoflagellate cysts in surface sediments from the North Atlantic Ocean and adjacent
801 seas in relation to sea-surface parameters: American Association of Stratigraphic
802 Palynologists Foundation Contributions Series 35, 150 pp.
- 803 Ruddiman, W.F., Raymo, M., McIntyre, A., 1986, Matuyama 41,000-year cycles: North
804 Atlantic Ocean and northern hemisphere ice sheets: *Earth and Planetary Science Letters* 80:
805 117-129.
- 806 Sangiorgi, F. & Donders, T.H., 2004. Reconstructing 150 years of eutrophication in the north-
807 western Adriatic Sea (Italy) using dinoflagellate cysts, pollen and spores. *Estuarine, Coastal*
808 *and Shelf Science* 60: 69-79.
- 809 Sangiorgi, F., Fabbri, D., Comandini, M., Gabbianelli, G. & Tagliavini, E., 2005. The
810 distribution of sterols and organic-walled dinoflagellate cysts in surface sediments of the
811 North-western Adriatic Sea (Italy). *Estuarine, Coastal and Shelf Science* 64: 395-406.
- 812 Seki, O., Foster, G.L., Schmidt, D.N., Mackensen, A., Kawamura, K., Pancost, R.D., 2010.
813 Alkenone and boron-based Pliocene pCO_2 records. *Earth and Planetary Science Letters* 292:
814 201-211. <http://dx.doi.org/10.1016/j.epsl.2010.01.037>.
- 815 Shackleton, N.J. and Hall, M.A., 1984. Oxygen and carbon isotope stratigraphy of Deep Sea
816 Drilling Project Hole 552A: Plio- Pleistocene glacial history. D-G. Roberts. D. Schnitker et al.
817 initial Reports of the Deep Sea Drilling Project 81: 599-609. U.S. Govt. Printing Office,
818 Washington.
- 819 Schreck, M., Meheust, M., Stein, R. and Matthiessen, J., 2013. Response of marine
820 palynomorphs to Neogene climate cooling in the Iceland Sea (ODP Hole 907A). *Marine*
821 *Micropaleontology* 101: 49-67.



- 822 Sinninghe Damsté, J.S., 2016. Spatial heterogeneity of sources of branched tetraethers in shelf
823 systems - The geochemistry of tetraethers in the Berau River delta (Kalimantan, Indonesia).
824 *Geochimica et Cosmochimica Acta* 186: 13-31.
- 825 Sluijs, A., Pross, J., and Brinkhuis, H., 2005. From greenhouse to icehouse; organic-walled
826 dinoflagellate cysts as paleoenvironmental indicators in the Paleogene: *Earth Science*
827 *Reviews* 68: 281-315.
- 828 Sørensen, J. C., Gregersen, U., Breiner, M. and O. Michelsen, 1997. High -frequency
829 sequence stratigraphy of Upper Cenozoic deposits in the central and southeastern North Sea
830 areas: *Marine and Petroleum Geology* 14 (2): 99-123.
- 831 Sosdian, S. Rosenthal, Y., 2009. Deep-sea temperature and ice volume changes across the
832 Pliocene-Pleistocene climate transitions. *Science* 325: 306-310. doi:10.1126/science.1169938
833 pmid:19608915.
- 834 Tabor, C.R., Poulsen, C.J., Pollard, D., 2014. Mending Milankovitch's theory: obliquity
835 amplification by surface feedbacks. *Climate of the Past*, 10, 41–50.
- 836 Thöle, H., Gaedicke, C., Kuhlmann, G., and Reinhardt, L., 2014. Late Cenozoic sedimentary
837 evolution of the German North Sea – A seismic stratigraphic approach. *Newsletters on*
838 *Stratigraphy* 47, 299–329.
- 839 Tzedakis, P.C., Crucifix, M., Mitsui, T., Wolff, E.W, 2017. A simple rule to determine which
840 insolation cycles lead to interglacials. *Nature* 542: 427–432, doi:10.1038/nature21364.
- 841 Svenning, J.-C., 2003. Deterministic Plio-Pleistocene extinctions in the European cool-
842 temperate tree flora. *Ecology Letters* 6: 646–653
- 843 Westerhoff, W., Donders, T.H. & Luthi, S.M., 2016. Report on ICDP workshop CONOSC
844 (COring the NOorth Sea Cenozoic). *Scientific Drilling* 21: 47-51.
- 845 Whitehead, D.R., (1983). Wind pollination: some ecological and evolutionary perspectives.
846 In: Real, L. (Ed.), *Pollination Biology*. Academic Press, Orlando, pp.
- 847 Williams, G.L., Fensome, R.A., and MacRae, R.A., 2017. The Lentin and Williams index of
848 fossil dinoflagellates 2004 edition. American Association of Stratigraphic Palynologists,
849 *Contributions Series* 48, College Station, TX, 1097 pp. 97–108
- 850 Van der Vlerk, I.M, Florschütz, F. 1953. The palaeontological base of the subdivision of the
851 Pleistocene in the Netherlands. *Verhandelingen Koninklijke Nederlandse Akademie van*
852 *Wetenschappen, Afdeling Natuurkunde*, 1e Reeks XX(2): 1–58.
- 853 Versteegh, G.J.M., Zonneveld, K.A.F., 1994. Determination of (palaeo-)ecological
854 preferences of dinoflagellates by applying detrended and canonical correspondence analysis
855 to late Pliocene dinoflagellate cyst assemblages of the south Italian Singha section. *Review of*
856 *Palaeobotany and Palynology* 84: 181–199.



- 857 Vonk, J.E., Gustafsson, Ö, 2009. Calibrating n-alkane *Sphagnum* proxies in sub-Arctic
858 Scandinavia. *Organic Geochemistry* 40: 1085-1090.
- 859 Zagwijn, W.H., 1960. Aspects of the Pliocene and early Pleistocene vegetation in The
860 Netherlands. *Mededelingen van de Geologische Stichting, Serie C III-1-5*, 1-78.
- 861 Zell, C., Kim, J.-H., Moreira-Turcq, P., Abril, G., Hopmans, E.C., Bonnet, M.-P., Sobrinho,
862 R. L., and Sinninghe Damsté, J.S., 2013. Disentangling the origins of branched tetraether
863 lipids and crenarchaeol in the lower Amazon River: implications for GDGT-based proxies,
864 *Limnology and Oceanography*. 58, 343-353.
- 865 Zhang, Z.-S., Nisancioglu, K. H., Chandler, M. A., Haywood, A. M., Otto-Bliesner, B. L.,
866 Ramstein, G., Stepanek, C., Abe-Ouchi, A., Chan, W.-L., Bragg, F. J., Contoux, C., Dolan, A.
867 M., Hill, D. J., Jost, A., Kamae, Y., Lohmann, G., Lunt, D. J., Rosenbloom, N. A., Sohl, L. E.,
868 and Ueda, H., 2013. Mid-pliocene Atlantic Meridional Overturning Circulation not unlike
869 modern. *Climate of the Past* 9, 1495-1504, doi:10.5194/cp-9-1495-2013
- 870 Ziegler, P.A., 1990. *Geological Atlas of Western and Central Europe (2nd edition)*. Shell
871 Internationale Petroleum Maatschappij B.V.; Geological Society Publishing House (Bath),
872 239 pp.
- 873 Zöllmer, V. and Irion, G., 1996. Tonminerale des Nordseeraumes ihr Verteilungsmuster in
874 kreidezeitlichen bis pleistozänen Sedimentabfolgen und in den Oberflächensedimenten der
875 heutigen Nordsee: Courier Forschungsinstitut Senckenberg, 190. Frankfurt am Mainz, 72 p.
- 876 Zonneveld, K.A.F., Marret, F., Versteegh, G.J.M., Bogus, K., Bonnet, S., Bouimetarhan, I.,
877 Crouch, E., de Vernal, A., Elshanawany, R., Edwards, L., Esper, O., Forke, S., Grøsfjeld, K.,
878 Henry, M., Holzwarth, U., Kieft, J.-F., Kim, S.-Y., Ladouceur, S., Ledu, D., Chen, L.,
879 Limoges, A., Londeix, L., Lu, S.-H., Mahmoud, M.S., Marino, G., Matsouka, K.,
880 Matthiessen, J., Mildenhall, D.C., Mudie, P., Neil, H.L., Pospelova, V., Qi, Y., Radi, T.,
881 Richerol, T., Rochon, A., Sangiorgi, F., Solignac, S., Turon, J.-L., Verleye, T., Wang, Y. &
882 Young, M., 2013. *Atlas of modern dinoflagellate cyst distribution based on 2405 data points*.
883 *Review of Palaeobotany and Palynology* 191: 1-197.
- 884